

pubs.acs.org/acsapm Forum Article

Functionalization of Benzotriazole-Based Conjugated Polymers for Solar Cells: Heteroatom vs Substituents

Jeromy James Rech, Liang Yan, Zhen Wang, Qianqian Zhang, Spencer Bradshaw, Harald Ade, and Wei You*



Cite This: ACS Appl. Polym. Mater. 2021, 3, 30-41



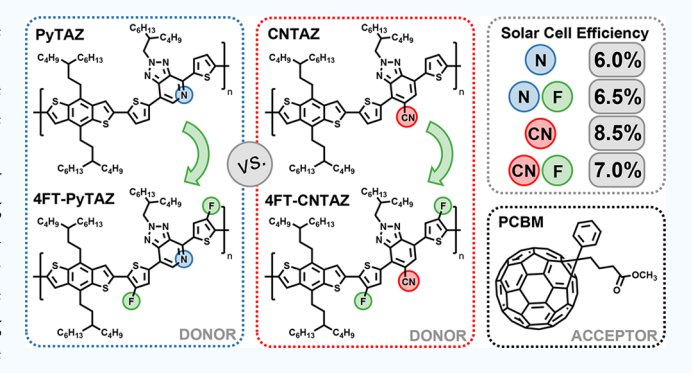
ACCESS

Metrics & More

Article Recommendations

Supporting Information

ABSTRACT: With the recent remarkable advances in the efficiency of organic solar cells, the need to distill key structure—property relationships for semiconducting materials cannot be understated. The fundamental design criteria based on these structure—property relationships will help realize low-cost, scalable, and high-efficiency materials. In this study, we systematically explore the impact of a variety of functional groups, including nitrogen heteroatoms, fluorine substituents, and cyano groups, on benzotriazole (TAZ)-based acceptor moieties that are incorporated into the conjugated polymers. Specifically, a pyridine heterocycle was used to replace the benzene unit of TAZ, leading to the PyTAZ polymer, and a cyano substituent was added to the benzene of the TAZ unit, resulting in the CNTAZ polymer. The



PyTAZ polymer suffers from low mobility and poor exciton harvesting, driven by large and excessively pure domains when blended with PCBM. The inclusion of fluorine substituents, placed strategically along the polymer backbone, can mitigate these issues, as shown with 4FT-PyTAZ. However, when this same approach is used for the cyano-functionalized polymer (CNTAZ), the resulting polymer (4FT-CNTAZ) is overfunctionalized and suffers from impure domains and recombination issues. The cyano group has a larger impact on the TAZ core compared to the nitrogen heteroatom due to the strong electron-withdrawing strength of the cyano group. Because of this, further functionalization of the cyano-based polymers has less fruitful impact on the polymer properties and results in deterioration of the solar cell efficiency. Overall, this work highlights some of the benefits, thresholds, and limitations for functionalization of conjugated polymers for organic solar cells.

KEYWORDS: organic photovoltaics, polymer solar cells, cyano substitution, conjugated polymers, nitrogen incorporation, structure—property relationship, fluorine substitution

1. INTRODUCTION

Organic solar cells (OSCs) based on semiconducting polymers offer a variety of advantages over traditional solar cell technologies, including the ability to create semitransparent, lightweight, and flexible solar panels through low-cost, solution-based processing.¹⁻⁷ The efficiency of organic solar cells is rapidly increasing, mainly driven by the creation of new materials; 8,9 however, the research community has devoted tremendous amount of efforts toward the structure-property relationship to make organic solar cells commercially viable by design. 10-15 These relationships include the impact of chemical structure on both the performance and long-term stability of the solar cell. 16-20 Our research lab, along with various others across the world, has worked on the synthesis of a large library of organic semiconducting polymers over the past decade; 1,3,21-23 however, many of these are missing key polymers to truly distill a complete ensemble of the structure property relationships.

One of the key chemical structures that we have worked extensively on is a benzotriazole (abbreviated as TAZ) acceptor moiety. The TAZ building block has unique and highly tunable features that make it appropriate for use in organic solar cells. For example, solubilizing side chains can be added selectively on the N-2 position of the triazole, which can allow for processability without inducing steric hindrance along the polymer backbone. The 5- and 6-positions (located on the "bottom" of the benzene farthest from the triazole) can be functionalized with a wide variety of substituents (such as fluorine, nitrogen, and cyano), which can further tune the polymer properties.²⁴ One of our most successful semi-

Special Issue: High Efficiency Polymers for Solar Cell Applications

Received: July 14, 2020 Accepted: September 4, 2020 Published: September 21, 2020





conducting materials is a copolymer with a benzodithiophene (BnDT) donor moiety and a fluorinated benzotriazole (FTAZ) acceptor moiety. ^{25,26} PBnDT-FTAZ (also commonly called FTAZ) achieved a high hole mobility on the order of 10⁻³ cm² V⁻¹ s⁻¹, and when paired with phenyl-C61-butyric acid methyl ester (PCBM), the resulting solar cell achieved over 7% efficiency. More recently with the advent of fused ring electron acceptors, FTAZ-based solar cells have achieved over 13% efficiency. 27,28 A summary of some of the structural variations of the TAZ core we have reported is shown in Figure S9, along with the solar cell efficiencies published with PCBM. ^{24,25,29–36} While we acknowledge that pairing many of these polymers with fused ring electron acceptors (such as ITIC³⁷ and Y6³⁸) can result in higher performance, this would increase the number of variables and make distilling meaningful structure-property relationships across publications difficult. Therefore, this work will only explore fullerenebased blends; yet, we anticipate that the new polymers reported here can offer improved efficiencies when paired with different acceptors. Nevertheless, from our current database of TAZ-based polymers, there are a series of unanswered questions that we intend to address in this work.

We recently published a series of TAZ-based polymers with varying amounts of cyano functionalization (zero = HTAZ, one = CNTAZ, and two = diCNTAZ).³² Unlike the trends we see with FTAZ, the addition of a second cyano group (diCNTAZ) results in a large decrease in the performance. In that work, we found that this degradation in performance upon addition of the second cyano group was driven by a decrease in the hole mobility and purity of domains, along with an increase in the recombination kinetics. This leads to our first set of questions: Is this decrease in performance upon further functionalization of cyano-functionalized polymers unique to only the cyano group? Or is a single cyano group the optimal amount of functionalization for the TAZ series?

Furthermore, while we have done a large variety of work with fluorination, the use of nitrogen heteroatoms was rather limited. In 2015, our group reported a pyridazine-based polymer (PrzTAZ); however, the efficiency was low (4.8%) primarily because of a poor hole mobility and fill factor. Interestingly, we also reported a pyridine-based polymer with an additional cyano substituent (PyCNTAZ), which demonstrated significantly higher efficiency (7.5%). This brings up the next set of questions: How does the performance of a pyridine-based TAZ core compare to the benzene- and pyridazine-based polymers? How does the method of nitrogen incorporation (i.e., nitrogen heteroatom vs cyano functional group) impact the polymer properties? Does the PrzTAZ polymer suffer from the same overfunctionalization issues as diCNTAZ?

And finally, we reported isomers of PBnDT-FTAZ, in which the fluorine substituents are moved from the TAZ acceptor moiety to the thiophene linkers connecting the BnDT and TAZ components (3FT-HTAZ and 4FT-HTAZ).³⁴ These publications have shown promise of fluorinated thiophene as structural units, but there are limited numbers of polymers on which they have been included. This leads to the final question: Can the incorporation of fluorine substituents on the thiophene linker result in improved solar cell performance for these new nitrogen-based functionalized acceptor moieties?

Each of these questions can be answered with a specific new series of conjugated polymers, which are shown in Chart 1. These include the pyridine-based polymers of PyTAZ and 4FT-PyTAZ and the cyano-functionalized CNTAZ and

Chart 1. Chemical Structures for the Four Polymers Used in This Study: PyTAZ, 4FT-PyTAZ, CNTAZ, and 4FT-CNTAZ

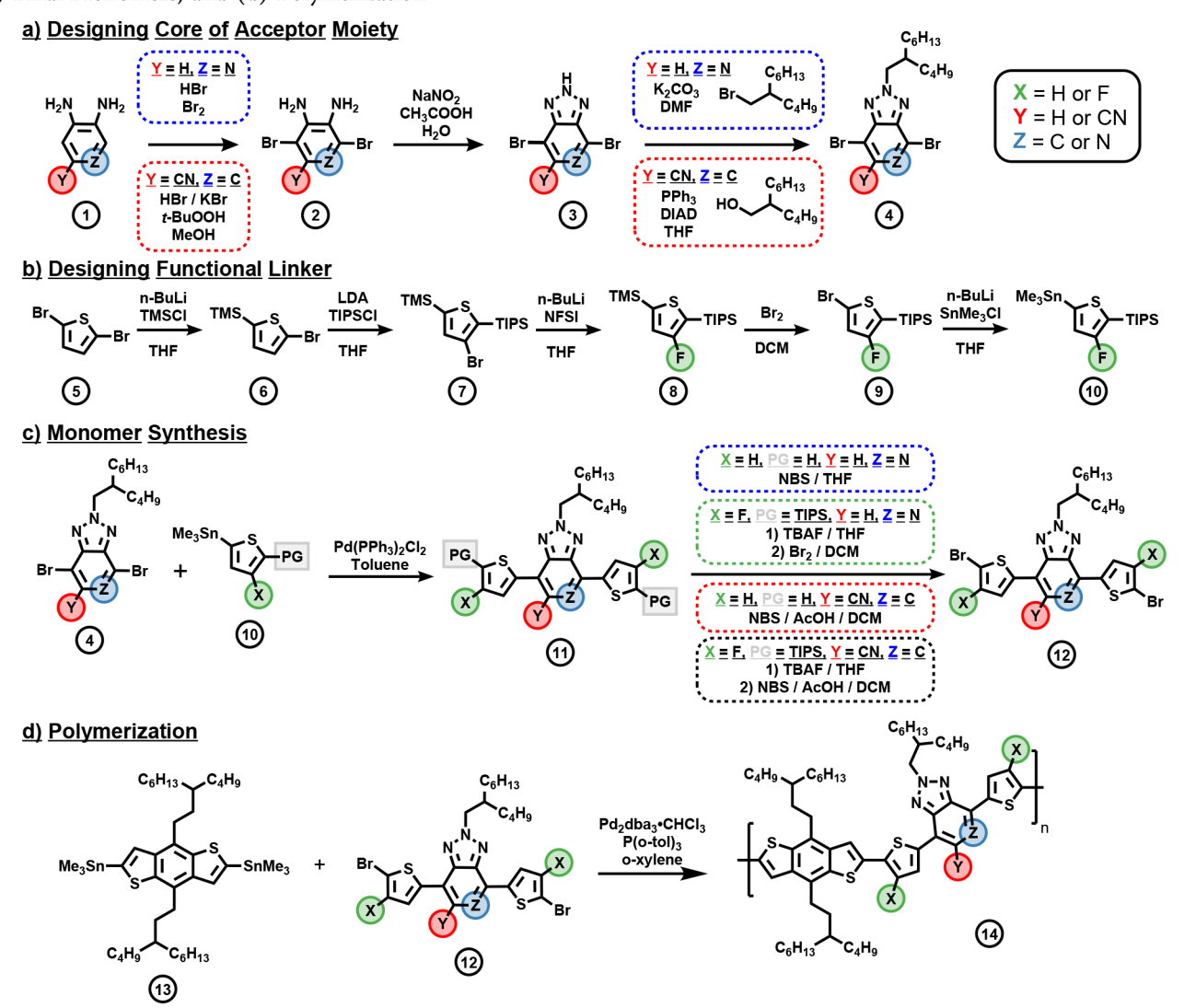
4FT-CNTAZ polymers. This series can offer further insight into the structure-property relationships of TAZ-based polymers and a deeper understanding to systems with various different types of functional groups as well as help design new materials in the future.

To create a detailed structure-property relationship, we investigated the optical, electrochemical, and photovoltaic properties of these polymers, and in order to understand the solar cell device results, we also explored the changes in morphology, charge-transfer state energy, and charge recombination dynamics. The PyTAZ polymer has an improved efficiency when paired with PCBM compared to HTAZ and PrzTAZ; however, trap-assisted recombination driven by a low mobility, large domain size, and excessively pure domain purity holds back the efficiency. The addition of the fluorine substituent (4FT-PyTAZ) results in a red-shifted UV-vis absorption and improved mobility. These changes are driven by the noncovalent intramolecular interactions, which result in a more planar backbone and closer π - π spacing. For the cyano-based polymers (CNTAZ and 4FT-CNTAZ), the stronger electron-withdrawing strength of the cyano group results in a red-shift and deeper HOMO energy levels. Furthermore, the cyano modification produced an improved voltage and current compared to the pyridine-based polymers. The 4FT-CNTAZ polymer has a decrease in efficiency compared to CNTAZ, but the magnitude of decrease is much smaller compared to diCNTAZ. The 4FT-CNTAZ is able to maintain a high open circuit voltage and hole mobility value, but a decrease in the domain purity and increase in charge carrier recombination—geminate recombination from low exciton splitting driving force—result in a loss of the shortcircuit current density and fill factor. Overall, this work highlights the key structure-property relationships with regards to nitrogen heteroatoms, cyano, and fluorine functional groups on TAZ-based semiconducting polymers used in organic solar cells.

2. RESULTS AND DISCUSSION

2.1. Synthesis. We began with the synthesis of the acceptor moiety core for both the PyTAZ and CNTAZ, shown in Scheme 1a. There are three fundamental steps, which

Scheme 1. Reaction Scheme for the Synthesis of the (a) Pyridine and Cyano-Based Acceptor Moieties, (b) Fluorinated Linker, (c) Final Monomers, and (d) Polymerization^a



"Some reaction arrows include various reaction conditions, denoted by the dashed boxes, based on the chemical identity of the starting material.

include (1) bromination of the aromatic core, (2) ring closure to form the triazole, and (3) addition of the solubilizing side chain. Normally, a different order is used when synthesizing TAZ-based monomers, in which bromination is the final step. For the PyTAZ and CNTAZ cores however, it is important to brominate prior to forming the triazole, as the electronwithdrawing nature of the triazole in addition to the new functional groups significantly increased the difficulty of the bromination. Specifically, after the triazole is formed (for both PyTAZ and CNTAZ), we tried a variety of brominating conditions, including very harsh conditions like refluxing for an entire week, and there was no appreciable amount of product formed. Therefore, to circumvent this issue, we used 3,4diaminopyridine and 3,4-diaminobenzonitrile (compound 1) as the starting materials for PyTAZ and CNTAZ, respectively. The pyridine-based substrate can undergo a straightforward bromination with hydrobromic acid and liquid bromine. However, for the cyano-substituted starting material, a more aggressive oxidative bromination with potassium bromide, hydrobromic acid, and tert-butyl hydroperoxide is needed to achieve compound 2. This bromination protocol has been

previously published by us and others. Following purification, compound 2 can be cyclized through conventional triazole chemistry to form compound 3. In the case of the PyTAZ core, the solubilizing side chain can be added through a standard alkylation reaction between the triazole and the brominated side chain; however, this same chemistry resulted in very poor yields on the CNTAZ substrate. Therefore, in order to synthesize compound 4 where Y = CN and Z = C, a Mitsunobu-type reaction was explored. In this reaction, the alcohol variant of the side chain is added with the assistance of triphenyl phosphine and diisopropyl azodicarboxylate (DIAD).

Next is the synthesis of the functional thiophene linker (4FT) for 4FT-PyTAZ and 4FT-CNTAZ. We have previously published a reaction scheme to a monofluorinated thiophene linker; however, that chemistry involved extra synthetic steps including a series of protection and deprotection reactions for the final compound to be fluorinated at the 4-position and stannylated at the 2-position. Furthermore, the starting material must be brominated on the 4-position, which increases the cost of the starting material by almost double. Here, we report a different synthetic route

Table 1. Molar Mass, Optical, and Electrochemical Properties of the Three Polymers

polymer	$M_{\rm n}$ (kg/mol)	Đ	$\lambda_{\text{max,sol}}$ (nm)	$\lambda_{\text{max,film}}$ (nm)	λ_{onset} (nm)	HOMO ^a (eV)	$LUMO^b$ (eV)	optical $E_{\rm gap}^{}$ (eV)
PyTAZ	34.3	2.6	550	549	639	-5.48	-3.54	1.94
			591	594				
4FT-PyTAZ	26.6	2.5	563	559	666	-5.64	-3.78	1.86
			606	607				
CNTAZ	44.7	2.4	564	565	664	-5.60	-3.72	1.87
			603	605				
4FT-CNTAZ	39.2	2.0	583	583	693	-5.66	-3.87	1.79
			623	625				

 a HOMO levels were estimated by cyclic voltammetry. b LUMO = HOMO + optical band gap. c Optical band gap was estimated from the onset of absorption of polymer films.

(Scheme 1b) to the same product that avoids these aforementioned issues. Starting with 2,5-dibromothiophene (compound 5), the first two reactions involve protection of the 2- and 5-positions of the thiophene linker. After 1 equiv of nbutyl lithium (n-BuLi) followed with chlorotrimethylsilane, the 2-position is protected with the TMS group. The next step utilizes a halogen dance rearrangement to protect the 5position while simultaneously moving the bromine to the 4position.⁴⁰ The choice of lithium disopropylamide (LDA) as the nucleophile is important, as it will lithiate the four position rather than removing the bromine, which is what n-BuLi would do. As the stability of the 4-position and 5-position of the thiophene differ, the halogen (bromine) and lithium would undergo a rearrangement to relocate the anion to the 5position, so upon addition of the electrophile/protecting group of chlorotriisopropylsilane, compound 7 is formed. Compound 8 is formed via electrophilic fluorination with N-fluorobenzenesulfonimide (NFSI). In order to increase the yield of this reaction, n-BuLi and NFSI were added in specific amounts over time; more details can be found in the Supporting Information. Finally, the 2-position, which is protected by TMS, can be selectively brominated and subsequently stannylated to form compound 10.

The stannylated thiophene linker and the brominated triazole core then undergo a Stille coupling reaction to form compound 11, which is the protected form of the final monomer. For PyTAZ and CNTAZ, there is no protecting group (i.e., PG = H), and the compound can be directly brominated. For 4FT-PyTAZ and 4FT-CNTAZ, the TIPS protecting group needs to first be removed with tetra-nbutylammonium fluoride (TBAF). The brominating conditions slightly vary for each of the substrates. PyTAZ can be brominated with N-bromosuccinimide (NBS), while a harsher reaction with liquid bromine is needed for 4FT-PyTAZ. Both of the CNTAZ-based compounds can undergo similar NBS bromination with the assistance of catalytic amounts of acetic acid. After compound 12 is made, the monomer is recrystallized multiple times to increase the purity to a level appropriate for polymerization. The BnDT monomer (compound 13) is synthesized according to previous reports.²

The conjugated polymers (PyTAZ, 4FT–PyTAZ, CNTAZ, and 4FT–CNTAZ) are made through a microwave-assisted, step growth, Stille polycondensation polymerization, ¹¹ shown in Scheme 1d. The ratio of compound 12 and compound 13 is varied to control the molar mass of the polymer through the Carothers equation. The number average molar mass ($M_{\rm n}$) and dispersity (D) of each polymer were measured through high-temperature gel permeation chromatography (HT-GPC), and the results are included in Table 1. All four of the resulting

polymers can be dissolved in common solvents used in OSCs, such as chloroform and chlorobenzene at elevated temperatures.

2.2. Optical and Electrochemical Properties. To investigate the impact of the structural changes on the optical and electrochemical properties, we first investigated the UVvis absorption of the polymers in a solution of 1,2,4trichlorobenzene (Figure 1a). The attenuation coefficients were also measured for thin films of each polymer and are depicted in Figure 1b; all of the polymers exhibit strong absorption in the visible region with similar attenuation coefficients slightly less than 1×10^5 cm⁻¹. The most notable differences between the four polymers optical properties occur at the longer wavelength region, which corresponds to the intramolecular charge-transfer (ICT) formation of the polymer backbones. Comparatively, the cyano-substituted polymers are red-shifted to the corresponding pyridine-containing polymers (CNTAZ vs PyTAZ, 4FT-CNTAZ vs 4FT-PyTAZ), and this shift is attributed to the stronger ICT formation due to the higher electron-withdrawing ability of the cyano group. The maximum absorption wavelengths and the absorption onset values for each polymer are included in Table 1.

Also, the addition of the fluorine on the thiophene linker results in a bathochromic shift of the UV-vis absorption by ~30 nm for both polymer types (CNTAZ vs 4FT-CTAZ, PyTAZ vs 4FT-PyTAZ). The fluorine induced red-shift is likely caused by the electron-withdrawing nature of fluorine coupled with noncovalent intramolecular interactions between the linker and neighboring core, which lead to a more planar backbone. There are a variety of reports demonstrating S···F interactions along the conjugated polymer backbones, 42-44 but we also confirmed this through computational modeling. We performed density functional theory (DFT) calculations at the DFT B3LYP/6-311+G(d) level of theory on one repeat unit for all four polymers, with the side chains reduced to an ethyl unit to reduce the complexity of the model. The results are included in Figure S10 along with energy level distributions (vide infra). In the nonfluorinated polymers (PyTAZ and CNTAZ), the dihedral angle between the BnDT unit and the thiophene linker is ~12°; upon addition of the fluorine, that same dihedral angle is drastically reduced toward zero. There are additional noncovalent planarizing interactions present in the PyTAZ series in the form of N···S interaction between the pyridine and neighboring thiophene. When Z = C (i.e., benzene core), the dihedral angle between the TAZ core and thiophene linker is around $2-3^{\circ}$, and when the carbon is replaced with a nitrogen to form the pyridine core, that same angle is reduced to 0°. A final note with the modeling involves the impact of the cyano substituent; while the cyano group is a

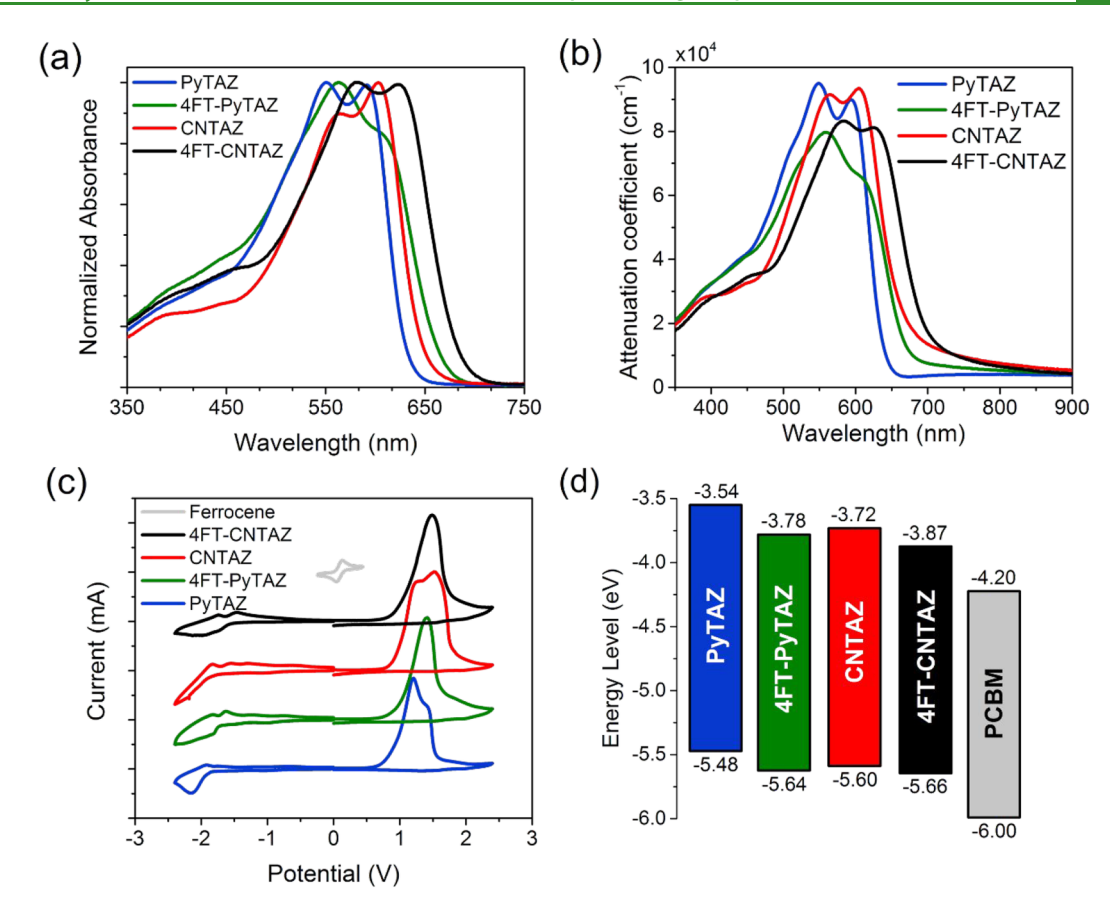


Figure 1. (a) Solution UV—vis for PyTAZ, 4FT—PyTAZ, CNTAZ, and 4FT—CNTAZ in trichlorobenzene, (b) thickness-normalized attenuation coefficient of thin polymer films measured via UV—vis, (c) cyclic voltammetry of polymer think films, and (d) resulting HOMO/LUMO energy level diagram for each polymer and PCBM.

very strong electron-withdrawing group, it is also bulkier than fluorine and increases the twisting of the backbone. The dihedral angle of the CNTAZ and 4FT–CNTAZ polymers about the cyano group increases from 2–3 to $\sim 30^{\circ}$ for both polymers. Fortunately, this steric impact does not negatively affect the mobility of the polymer, which is measured directly through space charge limited current (SCLC) measurements (Table 2).

Additionally, the UV—vis absorption spectra of the polymers in solution at room temperature are nearly identical to those of the thin film, which suggests that the polymer chains are already aggregated in the solution. The aggregation behavior of the polymers was also measured through temperature-dependent UV—vis absorption spectra in 1,2,4-trichlorobenzene between 20 and 120 °C (Figure S11). The most notable difference between the spectra of the four polymers is the change in aggregation strength upon fluorination. While PyTAZ (Figure S11a) and CNTAZ (Figure S11c) exhibit a complete loss of the far wavelength shoulder at elevated temperatures, 4FT—CNTAZ (Figure S11d) still includes the aggregation shoulder. This aligns with the modeling results, as the more planar backbones will have stronger interactions and thus aggregate.

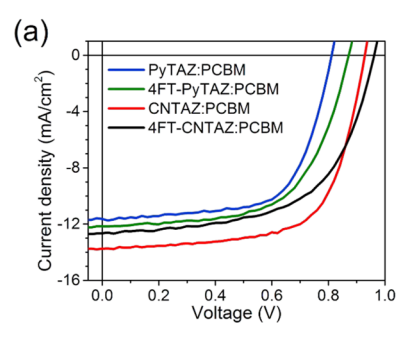
Finally, the electrochemical properties of the four polymers were measured through cyclic voltammetry (CV). A thin polymer film was deposited onto a glassy carbon working electrode, and the CV measurements were taken through a three-electrode configuration with the aforementioned working electrode, a Ag/Ag^+ reference electrode, and a platinum

counter electrode. The oxidation and reduction peaks for the three polymers are depicted in Figure 1c. The HOMO levels are estimated from the oxidation onset peak, in reference to a ferrocene/ferrocenium peak. The LUMO energy levels are estimated for each polymer through the optical band gap measured from the absorption onset of the UV—vis spectra and the HOMO. The DFT calculations also produce a value for the HOMO and LUMO energy values, which are included in Figure S10. Compared with the experimentally determined values, the values of energy levels from the calculations are all systematically shifted based on the assumptions made in the modeling; however, the same trends are seen among all four of the polymers. The corresponding highest occupied molecular orbital (HOMO) and lowest unoccupied molecular orbital (LUMO) energy levels for each polymer are shown in Figure

The CNTAZ HOMO energy level is 0.12 eV deeper than PyTAZ, because the cyano group is a stronger electron-withdrawing group, which is also consistent with the UV—vis results. This is advantageous as the open circuit voltage $(V_{\rm OC})$ is generally related to the energy difference between the LUMO of the acceptor (i.e., PCBM) and the HOMO of the donor polymer. Therefore, the CNTAZ-based polymers should exhibit an improved $V_{\rm OC}$ compared to the PyTAZ series. Next, when fluorine substituents are added to the polymer, the HOMO energy is also lowered from the electron-withdrawing nature of fluorine; however, the impact on the 4FT—PyTAZ polymer is different than on 4FT—CNTAZ. Between PyTAZ and 4FT—PyTAZ, there is a 0.16 eV decrease in the HOMO

Table 2. Photovoltaic Properties of the Various Polymer: PCBM Solar Cells

polymer	$J_{\rm SC}~({\rm mA/cm^2})$	$V_{\rm OC}$ (V)	FF (%)	PCE (%)	hole mobility ($\times 10^{-3} \text{ cm}^2/\text{V} \cdot \text{s}$)
PyTAZ	11.36 ± 0.49	0.809 ± 0.002	65.0 ± 0.8	5.98 ± 0.30	0.39
4FT-PyTAZ	11.85 ± 0.32	0.872 ± 0.001	62.4 ± 1.3	6.44 ± 0.23	0.56
CNTAZ	13.82 ± 0.32	0.926 ± 0.004	66.2 ± 1.0	8.48 ± 0.32	1.04
4FT-CNTAZ	12.63 ± 0.63	0.961 ± 0.001	57.4 ± 2.5	6.96 ± 0.18	1.08



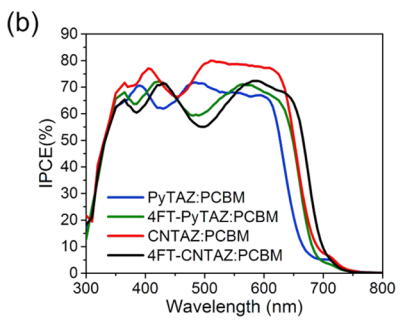


Figure 2. (a) Representative J-V curve and (b) IPCE curves of each OSC device.

energy level upon fluorination, but on the cyano series, this change in only 0.06 eV. This trend is consistent with our previous report, where we investigated cyano substitution; the addition of a second cyano group to form diCNTAZ only lowers the HOMO energy level by 0.02 eV.³² This diminishing return upon further functionalization occurs because while the substituent is electron-withdrawing, the acceptor moiety is already heavily electron-deficient, and the net impact of further functionalization is minimal.

2.3. Photovoltaic Properties. Next, these newly synthesized polymers were incorporated into bulk heterojunction (BHJ) solar cells with a conventional configuration of indium doped tin oxide (ITO)/copper(I) thiocyanate (CuSCN)/ polymer:PCBM/PFN/aluminum, where PFN stands for poly-[(9,9-bis(3'-(N,N-dimethylamino)propyl)-2,7-fluorene)-alt-2,7-(9,9-dioctylfluorene)]. 45 The active layer consisted of a 1:2 weight ratio of polymer:PCBM, and the thickness was kept to ~260 nm for all devices reported herein. The hole transport layer of CuSCN was selected because of the deep HOMO energy levels of the cyano-functionalized polymers. 46 A representative current density (J) vs voltage (\bar{V}) response for each solar cell is presented in Figure 2a. Similarly, the device characteristics of short-circuit current density (I_{SC}) , open circuit voltage (V_{OC}) , fill factor (FF), and power conversation efficiency (PCE) are summarized in Table 2, where each entry is the average of at least eight solar cells.

With regards to the structure—property relationship, the first clear trend is with $V_{\rm OC}$. Comparing the $V_{\rm OC}$ values for PyTAZ (0.809 V) and CNTAZ (0.926 V) polymers, the stronger electron-withdrawing strength from the cyano group results in a deeper HOMO energy level and thus a higher $V_{\rm OC}$. Similarly, with the fluorine impact, the $V_{\rm OC}$ increases between PyTAZ and 4FT—PyTAZ (0.809 to 0.872 V) and from CNTAZ to 4FT—CNTAZ (0.926 to 0.961 V). This is also consistent with the electrochemical properties highlighted previously, including the diminishing returns of further fluorination on flanking thiophenes (4FT) on the CNTAZ substrate compared to PyTAZ (0.06 V increase in the case of PyTAZ compared to 0.03 V for CNTAZ). While the electrochemical and photovoltaic properties present an overview, a more detailed investigation including measurements of the charge-transfer

(CT) state and $V_{\rm OC}$ loss of each blend was conducted (vide infra, Section 2.5).

Comparatively, the trends with J_{SC} are not as obvious. The addition of fluorine substituent in the form of 4FT to the PyTAZ core increases the current density (11.36 to 11.85 mA/ cm2 for 4FT-PyTAZ), which is a trend previously demonstrated with fluorination.³⁴ This increase in J_{SC} can be explained by the red-shift in absorption allowing for a wider range of photon harvesting coupled with the increase in hole mobility offered from the more planar backbone. The red-shift is also clear on the incident photon to charge carrier efficiency (IPCE) plot in Figure 2b. The CNTAZ exhibits the largest I_{SC} value of 13.82 mA/cm²; however, upon addition of the fluorine substituent, although the absorption red-shifts and the hole mobility is maintained, the 4FT-CNTAZ has a lower J_{SC} of only 12.63 mA/cm². This result dictates a further investigation to understand the loss mechanism for the current density in the 4FT-CNTAZ. Based on our previous results with diCNTAZ (benzotriazole core functionalized with two cyano groups), the addition of the second cyano group resulted in a degradation in device performance compared to CNTAZ, which was driven by a decrease in hole mobility, poor domain purity, and an increase in recombination kinetics.³² Interestingly, the hole mobility of 4FT-CNTAZ is actually marginally improved compared to that of CNTAZ. Therefore, the investigation was first to be directed to morphology (vide infra, Section 2.4) and then to the charge recombination dynamics (vide infra, Section 2.6).

As mentioned previously, the inclusion of two cyano groups in diCNTAZ resulted in poor domain purity compared to CNTAZ, and this unfavorable morphology resulted in a lower FF.³² Similarly, further functionalization of CNTAZ with fluorinated thiophene linkers (4FT) also decreases the FF from 66.2% for CNTAZ to 57.4% for 4FT–CNTAZ. When looking at the FF for the PyTAZ series, a similar effect, with less magnitude, is observed when comparing PyTAZ (65.0%) and 4FT–PyTAZ (62.4%). To confirm that the decrease in FF is from a morphological change, the morphology of each blend was explored (*vide infra*, Section 2.4).

Altogether, the combination of the $V_{\rm OC}$, $J_{\rm SC}$, and FF make up the PCE of the solar cell. Of the four polymers reported here, the PyTAZ exhibits the lowest efficiency of 5.98%. However,

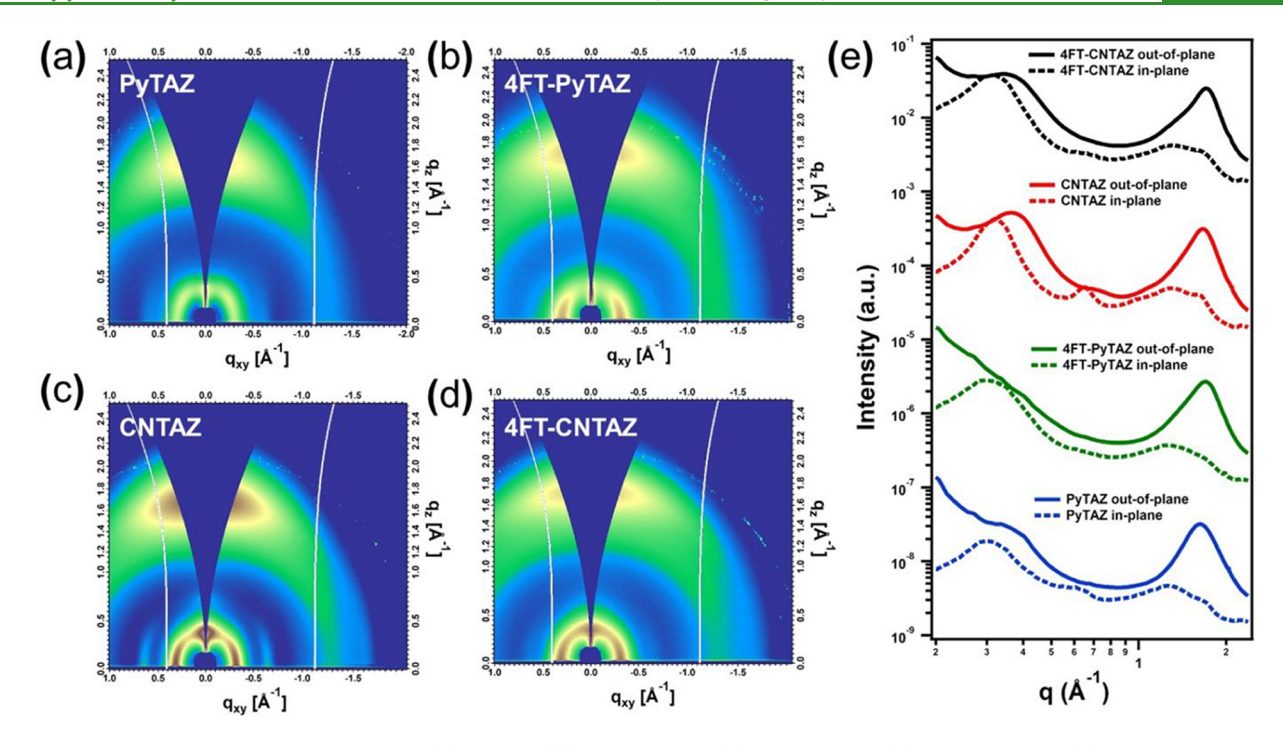


Figure 3. 2D GIWAXS patterns of neat films of (a) PyTAZ, (b) 4FT-PyTAZ, (c) CNTAZ, and (d) 4FT-CNTAZ. (e) 1D profiles for both in-plane (dashed) and out-of-plane (solid) directions.

compared to the unfunctionalized HTAZ (X = Y = H and Z =C) polymer, which has an efficiency of 4.39%, 25,35 the inclusion of the nitrogen heteroatom notably improved the efficiency. This increase in efficiency is driven by an increase in $V_{\rm OC}$, $I_{\rm SC}$, and FF, which highlights the value of the nitrogen heteroatom. Further functionalization of PyTAZ with fluorinated thiophene units (4FT) improved the J_{SC} and V_{OC} , and while there was a loss in FF, the overall efficiency of 4FT-PyTAZ is improved to 6.44%. Instead of incorporating the nitrogen group as a heteroatom, the stronger electronwithdrawing cyano group can achieve an even larger efficiency, with an average efficiency of 8.48% for CNTAZ. Further functionalization beyond one cyano group results in a degradation of performance. While 4FT-CNTAZ has an improved $V_{\rm OC}$, the loss in $J_{\rm SC}$ and FF results in a net lowering of the efficiency to 6.96%. As mentioned previously, to gain a more in-depth understanding of the structure-property relationship for this series of polymers, the morphology, charge-transfer energy, and charge recombination dynamics need to be explored.

2.4. Morphology and Fill Factor. The morphology of the active layer can be probed via synchrotron-radiation-based grazing incident wide-angle X-ray scattering (GIWAXS)⁴⁷ and resonant soft X-ray scattering (RSoXS).48 We first utilized GIWAXS to investigate the texture and packing of the polymers in both neat films (Figure 3) and blends with PCBM (Figure S12). First, all four neat polymers have some degree of preferential orientation. While all polymers exhibit a (010) $\pi - \pi$ stacking of peaks in the out-of-plane (OOP) direction, the strength of the (100) lamellar peaks in the inplane (IP) direction varies. A quantitative analysis would require pole-figure analysis taking the Ewald sphere correction into account. Qualitatively, 4FT-PyTAZ and 4FT-CNTAZ have the strongest face-on orientation, likely driven by the fluorine substituents. CNTAZ has both face-on and edge-on populations, with a larger population of the face-on

orientation. Finally, PyTAZ is the most weakly oriented. Face-on morphological arrangement is often beneficial to charge transport in OSCs, 49-51 which is also consistent with the higher mobility upon fluorination. There is also a trend in the π - π spacing upon fluorination; the 4FT-PyTAZ and 4FT-CNTAZ have (010) peaks in the OOP direction at higher q values than PyTAZ and CNTAZ. The larger reciprocal space values result in a smaller real space distances; thus, the fluorine substituent (i.e., 4FT) decreases the π - π stacking for both PyTAZ (3.85 to 3.70 Å) and CNTAZ (3.80 to 3.66 Å) series. This trend is also in good agreement with the computational and UV-vis results that suggest the fluorine can help planarize the backbone and allow for closer and stronger interactions between polymers. However, none of the polymers are semicrystalline (as processed) as the coherence lengths of the (010) peaks of the polymers, estimated from the Scherrer's equation, are similar and small (~2 nm), and the paracrystalline disorder parameter (g) is consistently high (\sim 17%) for all polymers, above the g-value of 12% of amorphous silicon. 52

When the various polymers were blended with PCBM to form the BHJ morphology, some of the differences are lost and characteristics are altered. The GIWAXS patterns (Figure S12) for the blend films show relative diffuse halos of both the PCBM and polymer diffraction features that cover both the OOP and IP directions, which represents a completely amorphous morphology. This is particularly the case for 4F-PyTAZ and 4F-CNTAZ with strong rings for (100) and (010), indicating a three-dimensional isotropic amorphous material. In contrast, PyTAZ and CNTAZ have simultaneously enhanced intensities for the (010) and (100) peaks, indicating a two-dimensional isotropic powder ("rolling log") with the polymer backbone preferentially in-plane but no other preferred orientation. The g-value of $\sim 13\%$ for each polymer also supports the disordered morphology. GIWAXS detects only the molecular packing of the samples, and if the neat films have poor packing, blending with a second component (i.e.,

Table 3. Morphological Features of Polymer Films and Polymer:PCBM Blends

polymer	(010) peak location ^a (\mathring{A}^{-1})	π - π stacking distance ^a (Å)	(010) peak coherence length ^a (Å)	$\begin{array}{c} long \ period^b \\ (nm) \end{array}$	relative RMS composition variation c
PyTAZ	1.63/1.68	3.85/3.74	14.7/45.2	49.8	1.00
4FT-PyTAZ	1.70/1.65	3.70/3.81	27.0/30.9	83.7/25.0	0.76
CNTAZ	1.65/1.62	3.80/3.87	17.0/34.2	27.2	0.77
4FT-CNTAZ	1.72/1.66	3.66/3.79	17.4/31.9	29.5	0.62

"In the format of a neat polymer/blend film. ^bApproximately equal to the spacing of like domains and roughly twice the domain size. ^cFormerly referred to as "relative domain purity", an imprecise notation.

Table 4. CT State Energy and the $V_{\rm oc}$ Loss of the Devices

polymer	$V_{\rm OC}$ (V)	$E_{\rm opt}^{a}$ (eV)	E_{CT} (eV)	$E_{\rm CT} - {\rm e}V_{\rm OC}~({\rm eV})$	$E_{\rm opt} - E_{\rm CT} \ ({\rm eV})$	total loss (eV)
PyTAZ	0.81	1.66	1.36	0.55	0.30	0.85
4FT-PyTAZ	0.87	1.66	1.52	0.65	0.14	0.79
CNTAZ	0.93	1.66	1.56	0.63	0.10	0.73
4FT-CNTAZ	0.96	1.66	1.59	0.63	0.07	0.70

^aThe smaller optical band gap (E_{opt}) of the two components, which is PCBM, is used.

PCBM) would normally worsen the packing. Therefore, RSoXS is used to better probe the blend film morphology (Figure S13). 48,55 The long periods (related to domain spacing) of the polymer:PCBM blends are generally similar for both CNTAZ and 4FT-CNTAZ (27.2 and 29.5 nm, respectively). The 4FT-PyTAZ:PCBM has two peaks that correspond to the pure acceptor phase and the mixed polymer phase (83.7 and 25 nm). Finally, the PyTAZ has a much larger domain with the long period of 49.8 nm, which can cause issues with charge separation.

The relative root-mean-square (RMS) variation of the composition is proportional to the integral of the scattering profiles over the length scale probed and is a widely used indicator related to the average domain purity of the OPV blends. 55,56 Domain purity is typically reflected in the FF value; impure domains lead to bimolecular recombination, and excessively pure domains can lead to isolated charge traps. 57-61 Of the four polymer blends measured here, PyTAZ:PCBM has the purest domain. The combination of the large domain size and excessively pure domain results in reduced efficiency of exciton harvesting, which explains why PyTAZ:PCBM has the lowest I_{SC} . The mechanism for this loss is presumably due to isolated charge traps based on the morphology; this will be further explored in the charge recombination dynamics section (vide infra, Section 2.6). Also, the 4FT-CNTAZ:PCBM blend has the most impure domain, which can explain the FF loss in the case of 4FT-CNTAZ when comparing CNTAZ and 4FT-CNTAZ. The molecular packing and morphological data from GIWAXS and RSoXS are summarized in Table 3.

2.5. CT State and V_{\rm OC} Loss. While $V_{\rm OC}$ trends can be predicted by the difference in the HOMO energy levels of the polymers, it is generally accepted that the $V_{\rm OC}$ is primarily determined by the energy of the interfacial charge-transfer (CT) state of the donor and the acceptor materials. ^{62–64} Vandewal and co-workers demonstrated that the CT state has a more direct relationship with $V_{\rm OC}$ through eq 1. ⁶⁵ Based on that same work, though less rigorous, the CT state ($E_{\rm CT}$) can be estimated by fitting high-sensitivity EQE measurements with eq 2. ⁶⁵ High-sensitivity EQE measurements and curve fittings for all four polymers can be found in Figure S14.

$$V_{\text{OC}} = \frac{kT}{q} \ln \left(\frac{J_{\text{ph}}}{J_0} + 1 \right)$$

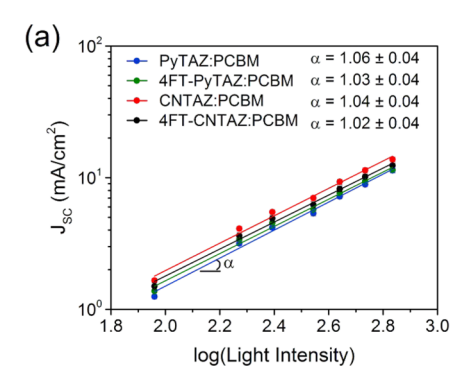
$$= \frac{E_{\text{CT}}}{q} + \frac{kT}{q} \ln \left(\frac{J_{\text{sc}} h^3 c^2}{fq 2\pi (E_{\text{CT}} - \lambda)} \right) + \frac{kT}{q} \ln (\text{EQE}_{\text{EL}})$$
(1)

$$EQE_{PV}(E) = \frac{f}{E\sqrt{4\pi\lambda kT}} \exp\left(\frac{-(E_{CT} + \lambda - E)^2}{4\lambda kT}\right)$$
(2)

Once the CT state is known, the mechanism for the $V_{\rm OC}$ can also be narrowed down. For example, the loss from nongeminate recombination can be found by finding the difference between the CT state energy and the $V_{\rm OC}$ (i.e., $E_{\rm CT}-eV_{\rm OC}$). Furthermore, another significant loss mechanism comes from the exciton splitting energy (also referred to as the charge separation energy), which is described as the difference between the optical band gap (PCBM in this case) and the charge-transfer state $(E_{\rm opt}-E_{\rm CT})$. Table 4 highlights these calculations detailing each of these loss mechanisms.

Similar to the claims made previously with regards to the HOMO energy levels, the cyano groups have a stronger electron-withdrawing strength and therefore lower the HOMO energy of the resulting polymer. The lower HOMO energy level results in a CT state higher than the PyTAZ-based polymers. The addition of the fluorine to the thiophene linker also raises the CT state energy; however, the impact on the PyTAZ polymer backbone is much larger than on CNTAZ (0.16 vs 0.03 eV), which again shows the diminishing returns on further functionalizing the CNTAZ polymer backbone.

Typical organic solar cells have similar nongeminate recombination values with loss values in the 0.5–0.7 eV range, which also holds true for the four polymers reported here. Furthermore, all of the blends have a $V_{\rm OC}$ loss to nongeminate recombination $(E_{\rm CT}-{\rm eV}_{\rm OC})$ of ~0.65 eV except for PyTAZ:PCBM, which is 0.1 eV lower. On the other hand, the required energy to split the exciton was estimated using $(E_{\rm opt}-E_{\rm CT})$. The cyano and fluorine substituents of 4FT–CNTAZ resulted in a polymer with a very low driving force for exciton splitting. While there have been recent reports with polymer blends that have both low exciton splitting energy and high exciton splitting efficiency, the lower driving force can result in increased geminate recombination and cause the decrease in $J_{\rm SC}$. This is likely the case for the $J_{\rm SC}$ loss in



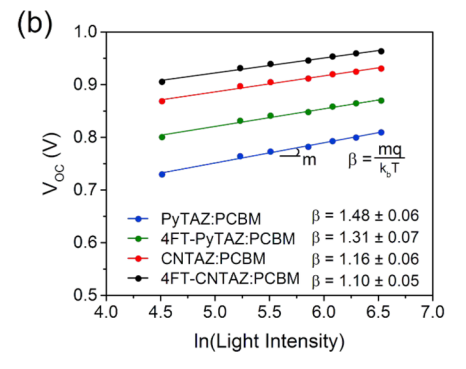


Figure 4. Light intensity measurements for (a) log-log fitting of I_{SC} vs light intensity and (b) semilog fitting of V_{OC} vs light intensity.

4FT-CNTAZ, which is also consistent with the trends seen in CNTAZ vs diCNTAZ.

2.6. Charge Recombination Dynamics. Finally, the mechanism for charge recombination was investigated through measuring J-V characteristics as a function of incident light intensity. It has been previously found that the slope of the log-log plot of $J_{\rm SC}$ vs light intensity can indicate the strength of bimolecular recombination under short-circuit conditions because of the power law dependence of $J_{\rm SC}$ on light intensity. As shown in Figure 4a, the slopes (α) for all four polymer blends are similar and close to 1. While the $J_{\rm SC}$ dependence does not yield any differences, the polymers blends have a very different response from the $V_{\rm OC}$ dependence.

In a semilog plot of $V_{\rm OC}$ vs light intensity (Figure 4b), the value of the slope (factored into β with k_bT/q) can provide what type of recombination is the major loss mechanism under open-circuit conditions. A $\beta = 2$ indicates that trap-assisted recombination is the dominant recombination mechanism, while β < 1 signifies that surface recombination is prevalent. PyTAZ:PCBM has the largest value (β = 1.48), which indicates an increase of trap-assisted recombination. This is consistent with the morphological data, which showed the PyTAZ:PCBM blends have the large and excessively pure domains, which can lead to isolated traps.⁵⁴ The addition of the fluorinated thiophene linker can help reduce the amount of trap-assisted recombination through a combination of a higher mobility, smaller domain size, and more appropriate domain purity. On the other hand, with β values close to 1, the cyano-functionalized polymers of CNTAZ and 4FT-CNTAZ do not appear to suffer from trap-assisted recombination, which results in the higher PCE.

3. CONCLUSION

In this study, we systematically explored various functionalization approaches on TAZ-based conjugated polymers that are used for organic solar cells. These approaches included the addition of nitrogen heteroatoms, fluorine substituents, and cyano groups along the polymer backbone. The Py-TAZ:PCBM blend had the worst performance of the four blends presented here. The weaker electronic effects of the nitrogen heteroatom limited the $V_{\rm OC}$, and trap-assisted recombination led to the lower $J_{\rm SC}$. The cause for the trap-assisted recombination originated from a lower hole mobility and a morphology of large and excessively pure domains. Including a fluorine substituent on the thiophene linkers of PyTAZ mitigated some of these issues and increased the solar cell efficiency. More specifically, the electron-withdrawing

nature of the fluorine atom can tune the energy levels and result in a higher $V_{\rm OC}$; furthermore, with a more planar backbone, 4FT-PyTAZ has a red-shift in absorption and higher mobility, which can boost the $I_{\rm SC}$.

As an alternative approach to incorporate nitrogen into the TAZ-based polymers, a cyano substituent can also be utilized. CNTAZ had the highest performance driven by the impact of the strong cyano electron-withdrawing group. In a hope to further improve the efficiency of the cyano-based polymers, the same fluorine approach was also explored to make 4FT-CNTAZ. While the $V_{\rm OC}$ showed improvements, our data show that the combination of two fluorines and one cyano per polymer repeat unit results in overfunctionalization of the polymer. Specifically, the 4FT-CNTAZ polymer has the lowest driving force for exciton splitting, which can result in geminate recombination; furthermore, the 4FT-CNTAZ:PCBM blends have impure domains, which result in FF loss. It is likely that one CN substituent is close to the optimal functionalization for TAZ-based polymers, since adding one additional CN was also detrimental to the device performance as previously reported by us with the diCNTAZ polymer. However, the field of cyano-based conjugated polymers is in its infancy compared to those of other functional groups like fluorine. Furthermore, there are even fewer reports that explore cyano-functionalized polymers with non-fullerene acceptors, and as non-fullerene acceptors have recently demonstrated remarkable efficiencies, a natural transition toward future improvement of these polymers involves pairing with appropriate non-fullerene acceptors. We anticipate that cyano-substituted polymers might offer excellent efficiencies when paired with non-fullerene acceptors and continue to push polymer solar cells toward commercialization.

Overall, this work contributes to the larger understanding of the structure—property relationships on TAZ-based polymers and also demonstrates the thresholds for functionalization. While using electron-withdrawing groups can offer great improvements in the solar cell efficiency, thresholds exist that can result in overfunctionalization and degradation in performance. Finally, non-fullerene acceptor blends that include cyano-functionalized polymers may offer a promising future direction of exploration of new high-efficiency organic solar cells.

ASSOCIATED CONTENT

Supporting Information

The Supporting Information is available free of charge at https://pubs.acs.org/doi/10.1021/acsapm.0c00761.

Synthetic details, ¹H NMR spectra and mass spectrometry, characterization methods, device fabrication details, thickness-dependent device results, summary of TAZ-based series, DFT calculations, temperature-dependent UV—vis spectroscopy, blend film GIWAXS, RSoXS profile, and high-sensitivity EQE fits (PDF)

AUTHOR INFORMATION

Corresponding Author

Wei You — Department of Chemistry, University of North Carolina at Chapel Hill, Chapel Hill, North Carolina 27599, United States; ⊙ orcid.org/0000-0003-0354-1948; Email: wyou@unc.edu

Authors

- Jeromy James Rech − Department of Chemistry, University of North Carolina at Chapel Hill, Chapel Hill, North Carolina 27599, United States; orcid.org/0000-0001-7963-9357
- Liang Yan Department of Chemistry, University of North Carolina at Chapel Hill, Chapel Hill, North Carolina 27599, United States; oocid.org/0000-0003-4122-7466
- **Zhen Wang** Department of Physics and Organic and Carbon Electronics Laboratories (ORaCEL), North Carolina State University, Raleigh, North Carolina 27695, United States
- Qianqian Zhang Department of Chemistry, University of North Carolina at Chapel Hill, Chapel Hill, North Carolina 27599, United States; occid.org/0000-0002-8896-1708
- **Spencer Bradshaw** Department of Chemistry, University of North Carolina at Chapel Hill, Chapel Hill, North Carolina 27599, United States
- Harald Ade Department of Physics and Organic and Carbon Electronics Laboratories (ORaCEL), North Carolina State University, Raleigh, North Carolina 27695, United States

Complete contact information is available at: https://pubs.acs.org/10.1021/acsapm.0c00761

Notes

The authors declare no competing financial interest.

ACKNOWLEDGMENTS

The authors thank NSF CBET-1639429 for financial support. Jianfei Qu and Feng He (Southern University of Science and Technology) are also acknowledged for running the hightemperature gel permeation chromatography measurements. We thank the University of North Carolina's Department of Chemistry Mass Spectrometry Core Laboratory, especially Diane Weatherspoon, for their assistance with mass spectrometry analysis. The Mass Spectrometry Core Lab is supported by the National Science Foundation under Grant No. CHE-1726291. We also like to thank Shubin Liu (University of North Carolina) for DFT calculations. GIWAXS measurements and analysis are supported by NSF (CBET-1639429). GIWAXS data were acquired at beamline 7.3.3, at the Advanced Light Source (ALS) in Berkeley National Lab, which is supported by the U.S. Department of Energy (No. DE-AC02-05CH11231).

REFERENCES

- (1) Wang, G.; Melkonyan, F. S.; Facchetti, A.; Marks, T. J. All-Polymer Solar Cells: Recent Progress, Challenges, and Prospects. *Angew. Chem., Int. Ed.* **2019**, 58 (13), 4129–4142.
- (2) Kippelen, B.; Brédas, J.-L. Organic Photovoltaics. *Energy Environ.* Sci. 2009, 2 (3), 251.

- (3) Zhou, H.; Yang, L.; You, W. Rational Design of High Performance Conjugated Polymers for Organic Solar Cells. *Macromolecules* **2012**, *45* (2), 607–632.
- (4) Kietzke, T. Recent Advances in Organic Solar Cells. Adv. OptoElectron. 2007, 2007, 1–15.
- (5) Ostroverkhova, O. Organic Optoelectronic Materials: Mechanisms and Applications. *Chem. Rev.* **2016**, *116* (22), 13279–13412.
- (6) Xu, G.; Shen, L.; Cui, C.; Wen, S.; Xue, R.; Chen, W.; Chen, H.; Zhang, J.; Li, H.; Li, Y.; Li, Y. High-Performance Colorful Semitransparent Polymer Solar Cells with Ultrathin Hybrid-Metal Electrodes and Fine-Tuned Dielectric Mirrors. *Adv. Funct. Mater.* 2017, 27 (15), 1605908.
- (7) Ravishankar, E.; Booth, R. E.; Saravitz, C.; Sederoff, H.; Ade, H. W.; O'Connor, B. T. Achieving Net Zero Energy Greenhouses by Integrating Semitransparent Organic Solar Cells. *Joule* **2020**, *4* (2), 490–506.
- (8) Cheng, P.; Li, G.; Zhan, X.; Yang, Y. Next-Generation Organic Photovoltaics Based on Non-Fullerene Acceptors. *Nat. Photonics* **2018**. *12* (3), 131–142.
- (9) Yan, C.; Barlow, S.; Wang, Z.; Yan, H.; Jen, A. K.-Y.; Marder, S. R.; Zhan, X. Non-Fullerene Acceptors for Organic Solar Cells. *Nat. Rev. Mater.* **2018**, 3 (3), 18003.
- (10) Baran, D.; Ashraf, R. S.; Hanifi, D. A.; Abdelsamie, M.; Gasparini, N.; Röhr, J. A.; Holliday, S.; Wadsworth, A.; Lockett, S.; Neophytou, M.; Emmott, C. J. M.; Nelson, J.; Brabec, C. J.; Amassian, A.; Salleo, A.; Kirchartz, T.; Durrant, J. R.; McCulloch, I. Reducing the Efficiency–Stability–Cost Gap of Organic Photovoltaics with Highly Efficient and Stable Small Molecule Acceptor Ternary Solar Cells. *Nat. Mater.* **2017**, *16* (3), 363–369.
- (11) Wadsworth, A.; Moser, M.; Marks, A.; Little, M. S.; Gasparini, N.; Brabec, C. J.; Baran, D.; McCulloch, I. Critical Review of the Molecular Design Progress in Non-Fullerene Electron Acceptors towards Commercially Viable Organic Solar Cells. *Chem. Soc. Rev.* **2019**, *48* (6), 1596–1625.
- (12) Polman, A.; Knight, M.; Garnett, E. C.; Ehrler, B.; Sinke, W. C. Photovoltaic Materials: Present Efficiencies and Future Challenges. *Science* **2016**, 352 (6283), aad4424.
- (13) Wang, G.; Adil, M. A.; Zhang, J.; Wei, Z. Large-Area Organic Solar Cells: Material Requirements, Modular Designs, and Printing Methods. *Adv. Mater.* **2019**, *31*, 1805089.
- (14) Zhang, M.; Guo, X.; Ma, W.; Ade, H.; Hou, J. A Large-Bandgap Conjugated Polymer for Versatile Photovoltaic Applications with High Performance. *Adv. Mater.* **2015**, *27* (31), 4655–4660.
- (15) Fan, Q.; Su, W.; Wang, Y.; Guo, B.; Jiang, Y.; Guo, X.; Liu, F.; Russell, T. P.; Zhang, M.; Li, Y. Synergistic Effect of Fluorination on Both Donor and Acceptor Materials for High Performance Non-Fullerene Polymer Solar Cells with 13.5% Efficiency. *Sci. China: Chem.* **2018**, *61* (5), 531–537.
- (16) Ghasemi, M.; Hu, H.; Peng, Z.; Rech, J. J.; Angunawela, I.; Carpenter, J. H.; Stuard, S. J.; Wadsworth, A.; McCulloch, I.; You, W.; Ade, H. Delineation of Thermodynamic and Kinetic Factors That Control Stability in Non-Fullerene Organic Solar Cells. *Joule* **2019**, 3 (5), 1328–1348.
- (17) Lee, H. K. H.; Telford, A. M.; Röhr, J. A.; Wyatt, M. F.; Rice, B.; Wu, J.; de Castro Maciel, A.; Tuladhar, S. M.; Speller, E.; McGettrick, J.; Searle, J. R.; Pont, S.; Watson, T.; Kirchartz, T.; Durrant, J. R.; Tsoi, W. C.; Nelson, J.; Li, Z. The Role of Fullerenes in the Environmental Stability of Polymer:Fullerene Solar Cells. *Energy Environ. Sci.* 2018, 11 (2), 417–428.
- (18) Jørgensen, M.; Norrman, K.; Gevorgyan, S. A.; Tromholt, T.; Andreasen, B.; Krebs, F. C. Stability of Polymer Solar Cells. *Adv. Mater.* **2012**, 24 (5), 580–612.
- (19) Mateker, W. R.; McGehee, M. D. Progress in Understanding Degradation Mechanisms and Improving Stability in Organic Photovoltaics. *Adv. Mater.* **2017**, *29* (10), 1603940.
- (20) Doumon, N. Y.; Wang, G.; Chiechi, R. C.; Koster, L. J. A. Relating Polymer Chemical Structure to the Stability of Polymer: Fullerene Solar Cells. *J. Mater. Chem. C* **2017**, 5 (26), 6611–6619.

- (21) Xiao, S.; Zhang, Q.; You, W. Molecular Engineering of Conjugated Polymers for Solar Cells: An Updated Report. *Adv. Mater.* **2017**, 29 (20), 1601391.
- (22) Yang, L.; Zhou, H.; Stuart, A. C.; You, W. Molecular Design of Conjugated Polymers for High-Efficiency Solar Cells 2014, 61–94.
- (23) Ma, Y.; Kang, Z.; Zheng, Q. Recent Advances in Wide Bandgap Semiconducting Polymers for Polymer Solar Cells. *J. Mater. Chem. A* **2017**, *5* (5), 1860–1872.
- (24) Li, W.; Yan, L.; Zhou, H.; You, W. A General Approach toward Electron Deficient Triazole Units to Construct Conjugated Polymers for Solar Cells. *Chem. Mater.* **2015**, 27 (18), 6470–6476.
- (25) Price, S. C.; Stuart, A. C.; Yang, L.; Zhou, H.; You, W. Fluorine Substituted Conjugated Polymer of Medium Band Gap Yields 7% Efficiency in Polymer-Fullerene Solar Cells. *J. Am. Chem. Soc.* **2011**, 133 (12), 4625–4631.
- (26) Roland, S.; Yan, L.; Zhang, Q.; Jiao, X.; Hunt, A.; Ghasemi, M.; Ade, H.; You, W.; Neher, D. Charge Generation and Mobility-Limited Performance of Bulk Heterojunction Solar Cells with a Higher Adduct Fullerene. J. Phys. Chem. C 2017, 121 (19), 10305–10316.
- (27) He, D.; Zhao, F.; Xin, J.; Rech, J. J.; Wei, Z.; Ma, W.; You, W.; Li, B.; Jiang, L.; Li, Y.; Wang, C. A Fused Ring Electron Acceptor with Decacyclic Core Enables over 13.5% Efficiency for Organic Solar Cells. Adv. Energy Mater. 2018, 8 (30), 1802050.
- (28) Ho, C. H. Y.; Kim, T.; Xiong, Y.; Firdaus, Y.; Yi, X.; Dong, Q.; Rech, J. J.; Gadisa, A.; Booth, R.; O'Connor, B. T.; Amassian, A.; Ade, H.; You, W.; Anthopoulos, T. D.; So, F. High-Performance Tandem Organic Solar Cells Using HSolar as the Interconnecting Layer. *Adv. Energy Mater.* 2020, *10*, 2000823.
- (29) Kelly, M. A.; Roland, S.; Zhang, Q.; Lee, Y.; Kabius, B.; Wang, Q.; Gomez, E. D.; Neher, D.; You, W. Incorporating Fluorine Substitution into Conjugated Polymers for Solar Cells: Three Different Means, Same Results. *J. Phys. Chem. C* **2017**, *121* (4), 2059–2068.
- (30) Chen, Z.; Yan, L.; Rech, J. J.; Hu, J.; Zhang, Q.; You, W. Green-Solvent-Processed Conjugated Polymers for Organic Solar Cells: The Impact of Oligoethylene Glycol Side Chains. *ACS Appl. Polym. Mater.* **2019**, *1* (4), 804–814.
- (31) Kelly, M. A.; Zhang, Q.; Peng, Z.; Noman, V.; Zhu, C.; Ade, H.; You, W. The Finale of a Trilogy: Comparing Terpolymers and Ternary Blends with Structurally Similar Backbones for Use in Organic Bulk Heterojunction Solar Cells. *J. Mater. Chem. A* **2018**, *6* (39), 19190–19200.
- (32) Zhang, Q.; Rech, J. J.; Yan, L.; Liang, Q.; Peng, Z.; Ade, H.; Wu, H.; You, W. Effect of Cyano Substitution on Conjugated Polymers for Bulk Heterojunction Solar Cells. ACS Appl. Polym. Mater. 2019, 1 (12), 3313–3322.
- (33) Bauer, N.; Zhang, Q.; Rech, J. J.; Dai, S.; Peng, Z.; Ade, H.; Wang, J.; Zhan, X.; You, W. The Impact of Fluorination on Both Donor Polymer and Non-Fullerene Acceptor: The More Fluorine, the Merrier. *Nano Res.* **2019**, *12* (9), 2400–2405.
- (34) Zhang, Q.; Yan, L.; Jiao, X.; Peng, Z.; Liu, S.; Rech, J. J.; Klump, E.; Ade, H.; So, F.; You, W. Fluorinated Thiophene Units Improve Photovoltaic Device Performance of Donor–Acceptor Copolymers. *Chem. Mater.* **2017**, *29* (14), 5990–6002.
- (35) Rech, J. J.; Yan, L.; Peng, Z.; Dai, S.; Zhan, X.; Ade, H.; You, W. Utilizing Difluorinated Thiophene Units To Improve the Performance of Polymer Solar Cells. *Macromolecules* **2019**, *52* (17), 6523–6532.
- (36) Uy, R. L.; Yan, L.; Li, W.; You, W. Tuning Fluorinated Benzotriazole Polymers through Alkylthio- Substitution and Selenophene Incorporation for Bulk. *Macromolecules* **2014**, 47 (7), 2289–2295
- (37) Lin, Y.; Zhan, X. Non-Fullerene Acceptors for Organic Photovoltaics: An Emerging Horizon. *Mater. Horiz.* **2014**, *1* (5), 470. (38) Yuan, J.; Zhang, Y.; Zhou, L.; Zhang, G.; Yip, H.-L.; Lau, T.-K.; Lu, X.; Zhu, C.; Peng, H.; Johnson, P. A.; Leclerc, M.; Cao, Y.; Ulanski, J.; Li, Y.; Zou, Y. Single-Junction Organic Solar Cell with over 15% Efficiency Using Fused-Ring Acceptor with Electron-Deficient Core. *Joule.* **2019**, *3*, 1140.

- (39) Wudarczyk, J.; Papamokos, G.; Margaritis, V.; Schollmeyer, D.; Hinkel, F.; Baumgarten, M.; Floudas, G.; Müllen, K. Hexasubstituted Benzenes with Ultrastrong Dipole Moments. *Angew. Chem., Int. Ed.* **2016**, *55* (9), 3220–3223.
- (40) Schnürch, M.; Spina, M.; Khan, A. F.; Mihovilovic, M. D.; Stanetty, P. Halogen Dance Reactions—A Review. *Chem. Soc. Rev.* **2007**, *36* (7), 1046–1057.
- (41) Li, W.; Yang, L.; Tumbleston, J. R.; Yan, L.; Ade, H.; You, W. Controlling Molecular Weight of a High Efficiency Donor-Acceptor Conjugated Polymer and Understanding Its Significant Impact on Photovoltaic Properties. *Adv. Mater.* **2014**, *26* (26), 4456–4462.
- (42) Huang, H.; Yang, L.; Facchetti, A.; Marks, T. J. Organic and Polymeric Semiconductors Enhanced by Noncovalent Conformational Locks. *Chem. Rev.* **2017**, *117* (15), 10291–10318.
- (43) Thorley, K. J.; McCulloch, I. Why Are S-F and S-O Non-Covalent Interactions Stabilising? *J. Mater. Chem. C* **2018**, 6 (45), 12413–12421.
- (44) Cheng, Y.; Qi, Y.; Tang, Y.; Zheng, C.; Wan, Y.; Huang, W.; Chen, R. Controlling Intramolecular Conformation through Nonbonding Interaction for Soft-Conjugated Materials: Molecular Design and Optoelectronic Properties. *J. Phys. Chem. Lett.* **2016**, 7 (18), 3609–3615.
- (45) Hamilton, R.; Shuttle, C. G.; O'Regan, B.; Hammant, T. C.; Nelson, J.; Durrant, J. R. Recombination in Annealed and Nonannealed Polythiophene/Fullerene Solar Cells: Transient Photovoltage Studies versus Numerical Modeling. *J. Phys. Chem. Lett.* **2010**, *1* (9), 1432–1436.
- (46) Pattanasattayavong, P.; Yaacobi-Gross, N.; Zhao, K.; Ndjawa, G. O. N.; Li, J.; Yan, F.; O'Regan, B. C.; Amassian, A.; Anthopoulos, T. D. Hole-Transporting Transistors and Circuits Based on the Transparent Inorganic Semiconductor Copper(I) Thiocyanate (CuSCN) Processed from Solution at Room Temperature. *Adv. Mater.* **2013**, 25 (10), 1504–1509.
- (47) Hexemer, A.; Bras, W.; Glossinger, J.; Schaible, E.; Gann, E.; Kirian, R.; MacDowell, A.; Church, M.; Rude, B.; Padmore, H. A SAXS/WAXS/GISAXS Beamline with Multilayer Monochromator. *J. Phys. Conf. Ser.* **2010**, 247, 012007.
- (48) Gann, E.; Young, A. T.; Collins, B. A.; Yan, H.; Nasiatka, J.; Padmore, H. A.; Ade, H.; Hexemer, A.; Wang, C. Soft X-Ray Scattering Facility at the Advanced Light Source with Real-Time Data Processing and Analysis. *Rev. Sci. Instrum.* **2012**, 83 (4), 045110.
- (49) Duan, C.; Gao, K.; van Franeker, J. J.; Liu, F.; Wienk, M. M.; Janssen, R. A. J. Toward Practical Useful Polymers for Highly Efficient Solar Cells via a Random Copolymer Approach. *J. Am. Chem. Soc.* **2016**, *138* (34), 10782–10785.
- (50) Yao, H.; Li, Y.; Hu, H.; Chow, P. C. Y.; Chen, S.; Zhao, J.; Li, Z.; Carpenter, J. H.; Lai, J. Y. L.; Yang, G.; Liu, Y.; Lin, H.; Ade, H.; Yan, H. A Facile Method to Fine-Tune Polymer Aggregation Properties and Blend Morphology of Polymer Solar Cells Using Donor Polymers with Randomly Distributed Alkyl Chains. Adv. Energy Mater. 2018, 8 (6), 1701895.
- (51) Li, S.; Ye, L.; Zhao, W.; Liu, X.; Zhu, J.; Ade, H.; Hou, J. Design of a New Small-Molecule Electron Acceptor Enables Efficient Polymer Solar Cells with High Fill Factor. *Adv. Mater.* **2017**, 29 (46), 1704051.
- (52) Rivnay, J.; Noriega, R.; Kline, R. J.; Salleo, A.; Toney, M. F. Quantitative Analysis of Lattice Disorder and Crystallite Size in Organic Semiconductor Thin Films. *Phys. Rev. B: Condens. Matter Mater. Phys.* **2011**, 84 (4), 045203.
- (53) Peng, Z.; Ye, L.; Ade, H. Understanding, Quantifying, and Controlling the Molecular Ordering of Semi-Conducting Polymers: From Novices to Experts and Amorphous to Perfect Crystals. *arXiv*, May 27, 2020. https://arxiv.org/abs/2005.13155.
- (54) Bartelt, J. A.; Beiley, Z. M.; Hoke, E. T.; Mateker, W. R.; Douglas, J. D.; Collins, B. A.; Tumbleston, J. R.; Graham, K. R.; Amassian, A.; Ade, H.; Fréchet, J. M. J.; Toney, M. F.; McGehee, M. D. The Importance of Fullerene Percolation in the Mixed Regions of Polymer-Fullerene Bulk Heterojunction Solar Cells. *Adv. Energy Mater.* 2013, 3 (3), 364–374.

- (55) Collins, B. A.; Li, Z.; Tumbleston, J. R.; Gann, E.; Mcneill, C. R.; Ade, H. Absolute Measurement of Domain Composition and Nanoscale Size Distribution Explains Performance in PTB7:PC71bm Solar Cells. *Adv. Energy Mater.* **2013**, 3 (1), 65–74.
- (56) Ye, L.; Stuard, S. J.; Ade, H. Soft X-Ray Scattering Characterization of Polymer Semiconductors. *Conjugated Polymers* **2019**, 427–458.
- (57) Ye, L.; Hu, H.; Ghasemi, M.; Wang, T.; Collins, B. A.; Kim, J.-H.; Jiang, K.; Carpenter, J. H.; Li, H.; Li, Z.; McAfee, T.; Zhao, J.; Chen, X.; Lai, J. L. Y.; Ma, T.; Bredas, J.-L.; Yan, H.; Ade, H. Quantitative Relations between Interaction Parameter, Miscibility and Function in Organic Solar Cells. *Nat. Mater.* **2018**, *17* (3), 253–260.
- (58) Ye, L.; Zhao, W.; Li, S.; Mukherjee, S.; Carpenter, J. H.; Awartani, O.; Jiao, X.; Hou, J.; Ade, H. High-Efficiency non-fullerene Organic Solar Cells: Critical Factors That Affect Complex Multi-Length Scale Morphology and Device Performance. *Adv. Energy Mater.* **2017**, 7 (7), 1602000.
- (59) Mukherjee, S.; Jiao, X.; Ade, H. Charge Creation and Recombination in Multi-Length Scale Polymer:Fullerene BHJ Solar Cell Morphologies. *Adv. Energy Mater.* **2016**, *6* (18), 1600699.
- (60) Ma, W.; Ye, L.; Zhang, S.; Hou, J.; Ade, H. Competition between Morphological Attributes in the Thermal Annealing and Additive Processing of Polymer Solar Cells. *J. Mater. Chem. C* **2013**, *1* (33), 5023.
- (61) Ma, W.; Tumbleston, J. R.; Wang, M.; Gann, E.; Huang, F.; Ade, H. Domain Purity, Miscibility, and Molecular Orientation at Donor/Acceptor Interfaces in High Performance Organic Solar Cells: Paths to Further Improvement. *Adv. Energy Mater.* **2013**, 3 (7), 864–872.
- (62) Wang, T.; Chen, X.-K.; Ashokan, A.; Zheng, Z.; Ravva, M. K.; Brédas, J.-L. Bulk Heterojunction Solar Cells: Impact of Minor Structural Modifications to the Polymer Backbone on the Polymer-Fullerene Mixing and Packing and on the Fullerene-Fullerene Connecting Network. *Adv. Funct. Mater.* 2018, 28 (14), 1705868.
- (63) Tang, A.; Xiao, B.; Wang, Y.; Gao, F.; Tajima, K.; Bin, H.; Zhang, Z.-G.; Li, Y.; Wei, Z.; Zhou, E. Simultaneously Achieved High Open-Circuit Voltage and Efficient Charge Generation by Fine-Tuning Charge-Transfer Driving Force in Nonfullerene Polymer Solar Cells. *Adv. Funct. Mater.* **2018**, 28 (6), 1704507.
- (64) Athanasopoulos, S.; Schauer, F.; Nádaždy, V.; Weiß, M.; Kahle, F.; Scherf, U.; Bässler, H.; Köhler, A. What Is the Binding Energy of a Charge Transfer State in an Organic Solar Cell? *Adv. Energy Mater.* **2019**, *9* (24), 1900814.
- (65) Vandewal, K.; Tvingstedt, K.; Gadisa, A.; Inganäs, O.; Manca, J. V. Relating the Open-Circuit Voltage to Interface Molecular Properties of Donor:Acceptor Bulk Heterojunction Solar Cells. *Phys. Rev. B: Condens. Matter Mater. Phys.* **2010**, *81* (12), 125204.
- (66) Faist, M. A.; Kirchartz, T.; Gong, W.; Ashraf, R. S.; McCulloch, I.; de Mello, J. C.; Ekins-Daukes, N. J.; Bradley, D. D. C.; Nelson, J. Competition between the Charge Transfer State and the Singlet States of Donor or Acceptor Limiting the Efficiency in Polymer:-Fullerene Solar Cells. J. Am. Chem. Soc. 2012, 134 (1), 685–692.
- (67) Hoke, E. T.; Vandewal, K.; Bartelt, J. A.; Mateker, W. R.; Douglas, J. D.; Noriega, R.; Graham, K. R.; Fréchet, J. M. J.; Salleo, A.; McGehee, M. D. Recombination in Polymer:Fullerene Solar Cells with Open-Circuit Voltages Approaching and Exceeding 1.0 V. Adv. Energy Mater. 2013, 3 (2), 220–230.
- (68) Koster, L. J. A.; Kemerink, M.; Wienk, M. M.; Maturová, K.; Janssen, R. A. J. Quantifying Bimolecular Recombination Losses in Organic Bulk Heterojunction Solar Cells. *Adv. Mater.* **2011**, 23 (14), 1670–1674.
- (69) Stolterfoht, M.; Armin, A.; Philippa, B.; White, R. D.; Burn, P. L.; Meredith, P.; Juška, G.; Pivrikas, A. Photocarrier Drift Distance in Organic Solar Cells and Photodetectors. *Sci. Rep.* **2015**, 5 (1), 9949. (70) Würfel, U.; Perdigón-Toro, L.; Kurpiers, J.; Wolff, C. M.; Caprioglio, P.; Rech, J. J.; Zhu, J.; Zhan, X.; You, W.; Shoaee, S.; Neher, D.; Stolterfoht, M. Recombination between Photogenerated and Electrode-Induced Charges Dominates the Fill Factor Losses in

- Optimized Organic Solar Cells. J. Phys. Chem. Lett. 2019, 10 (12), 3473-3480.
- (71) Cowan, S. R.; Roy, A.; Heeger, A. J. Recombination in Polymer-Fullerene Bulk Heterojunction Solar Cells. *Phys. Rev. B: Condens. Matter Mater. Phys.* **2010**, 82 (24), 245207.
- (72) Tress, W.; Yavari, M.; Domanski, K.; Yadav, P.; Niesen, B.; Correa Baena, J. P.; Hagfeldt, A.; Graetzel, M. Interpretation and Evolution of Open-Circuit Voltage, Recombination, Ideality Factor and Subgap Defect States during Reversible Light-Soaking and Irreversible Degradation of Perovskite Solar Cells. *Energy Environ. Sci.* **2018**, *11* (1), 151–165.